

Distance-Dependent Electron Transfer Kinetics in Axially Connected Silicon Phthalocyanine-Fullerene Conjugates

Luis Martín-Gomis, [a] Sairaman Seetharaman⁺, [b] David Herrero⁺, [a] Paul A. Karr, [c] Fernando Fernández-Lázaro, [a] Francis D'Souza, *[b] and Ángela Sastre-Santos *[a]

Dedicated to Professor Karl M. Kadish on the occasion of his 75th birthday

The effect of donor-acceptor distance in controlling the rate of electron transfer in axially linked silicon phthalocyanine-C₆₀ dyads has been investigated. For this, two C₆₀-SiPc-C₆₀ dyads, 1 and 2, varying in their donor-acceptor distance, have been newly synthesized and characterized. In the case of C₆₀-SiPc-C₆₀ 1 where the SiPc and C₆₀ are separated by a phenyl spacer, faster electron transfer was observed with k_{cs} equal to 2.7× $10^9 \,\mathrm{s}^{-1}$ in benzonitrile. However, in the case of C_{60} -SiPc- C_{60} 2, where SiPc and C₆₀ are separated by a biphenyl spacer, a slower electron transfer rate constant, $k_{cs} = 9.1 \times 10^8 \text{ s}^{-1}$, was recorded. The addition of an extra phenyl spacer in 2 increased the donor-acceptor distance by ~4.3 Å, and consequently, slowed down the electron transfer rate constant by a factor of ~3.7. The charge separated state lasted over 3 ns, monitoring time window of our femtosecond transient spectrometer. Complimentary nanosecond transient absorption studies revealed formation of ³SiPc* as the end product and suggested the final lifetime of the charge separated state to be in the 3-20 ns range. Energy level diagrams established to comprehend these mechanistic details indicated that the comparatively highenergy SiPc*+-C₆₀*- charge separated states (1.57 eV) populated the low-lying ³SiPc* (1.26 eV) prior returning to the ground state.

1. Introduction

We, as a modern society, are heavily dependent on depleting non-renewable sources like fossil fuels to meet our energy demands. There is a real need to shift our focus towards more clean and renewable energy sources. Sunlight is one of the freely available sources of energy that has an enormous potential to be utilized to meet our constant energy demands. However, there is an immense gap when it comes to utilizing solar energy in comparison to abundant source of sunlight that reaches our planet. Through photosynthesis, plants have demonstrated that there is a tremendous scope to harvest light energy from the sun. Artificial photosynthesis is an evergrowing field where new molecular systems have been studied to create ideal models that can replace the current generation of photovoltaics.[1-3]

Multichromophoric systems consisting of donor-acceptor assemblies are of great significance in designing new molecular architectures for artificial photosynthesis.[4-20] To investigate their potential use in artificial photosynthesis, these molecular building blocks should demonstrate novel photophysical characteristics including high tunability in the UV-Vis spectrum and the ability to harvest sunlight. Porphyrinoid electron-donor, usually porphyrins and phthalocyanines, are preferred for building artificial photosynthetic systems, due to their high molar extinction coefficients and photo-tunability. [21,22] On the other hand, C₆₀-fullerene, the well-known electron acceptor, is often preferred due to its low reorganization energy making it an ideal candidate for donor-acceptor molecular systems. [23] Furthermore, upon reduction, C_{60} containing systems tend to show faster charge separation and slower recombination processes, such property is important in building constructs which behave close to photosynthetic pigments for efficient light harvesting. [24] That is why donor-acceptor arrangements based on porphyrin/phthalocyanine and C₆₀-fullerene, represent an outstanding majority. [25-33]

In the context of donor-acceptor design, there are few examples of covalent multimodular artificial photosynthetic systems, where electron-acceptor units are arranged in the axial positions of a suitable porphyrinoid macrocycle, thus providing molecular systems that undergo photo-induced electron transfer processes in a very efficient way.[19,34-45] One of the most versatile building-blocks is silicon phthalocyanine (SiPc), which can be easily functionalized at axial positions through a variety of functionalities. Our groups have experience in syntheses and

- [a] Dr. L. Martín-Gomis, D. Herrero, Prof. Dr. F. Fernández-Lázaro, Prof. Dr. Á. Sastre-Santos División de Química Orgánica, Instituto de Bioingeniería Universidad Miguel Hernández Avda. de la Universidad s/n 03203 Elche (Spain)
- E-mail: asastre@umh.es [b] S. Seetharaman, Prof. Dr. F. D'Souza Department of Chemistry University of North Texas at Denton 1155 Union Circle, #305070, Denton, TX 76203-5017 (USA) E-mail: Francis.DSouza@unt.edu
- [c] Prof. Dr. P. A. Karr Department of Physical Sciences and Mathematics Wayne State College 1111 Main Street, Wayne, Nebraska 68787 (USA)
- [+] These authors contributed equally to this work.
 - Supporting information for this article is available on the WWW under https://doi.org/10.1002/cphc.202000578

Wiley Online Library



photophysical study of SiPc-based donor-acceptor arrangements. To name a few, axially functionalized SiPc macrocycles with trinitrofluorene (TNF),[46] perylenediimide nanotubes, $^{[48]}$ or fullerenes ($C_{59}N$ and C_{60}), $^{[16,49]}$ and combinations of them, [50] demonstrate the tunability and potential of these systems in the field of artificial photosynthesis.

It is worth highlighting two different SiPc compounds, asymmetrically and axially functionalized with both perylenediimide (PDI) and fulleropyrrolidine electroactive units, recently published by our research groups. [51,52] Analyzing both works together, we concluded that, to efficiently obtain long-lived charged separated states, it is preferable to have only fullerene-C₆₀ subunits in the axial positions of an electron-rich SiPc moiety, wherein the distance should be fixed through adequate-length rigid connectors. Here, we present the synthesis, characterization and evaluation of their photophysical properties of a series of triads (C₆₀-SiPc-C₆₀ 1 and 2) where a SiPc unit, specially designed to present an improved electron donating character, with eight 2,6-dimethylphenoxyl groups arranged in the peripheral positions, is combined, in a covalent manner, with two fullerene-C₆₀ appends. These appends are symmetrically located in the axial positions of the central silicon atom, and the distance to the phthalocyanine core is varied through conjugated rigid connectors of different lengths (Figure 1). This work constitutes one of the few examples of systematic study about the influence of the distance between electroactive units

C₆₀-SiPc-C₆₀ 1 C₆₀-SiPc-C₆₀ 2

Figure 1. Molecular structure of C₆₀-SiPc-C₆₀ 1 and C₆₀-SiPc-C₆₀ 2 investigated in the present study.

on the photophysical properties of systems based on SiPc and C₆₀, for their application as artificial photosynthetic systems.

2. Results and Discussion

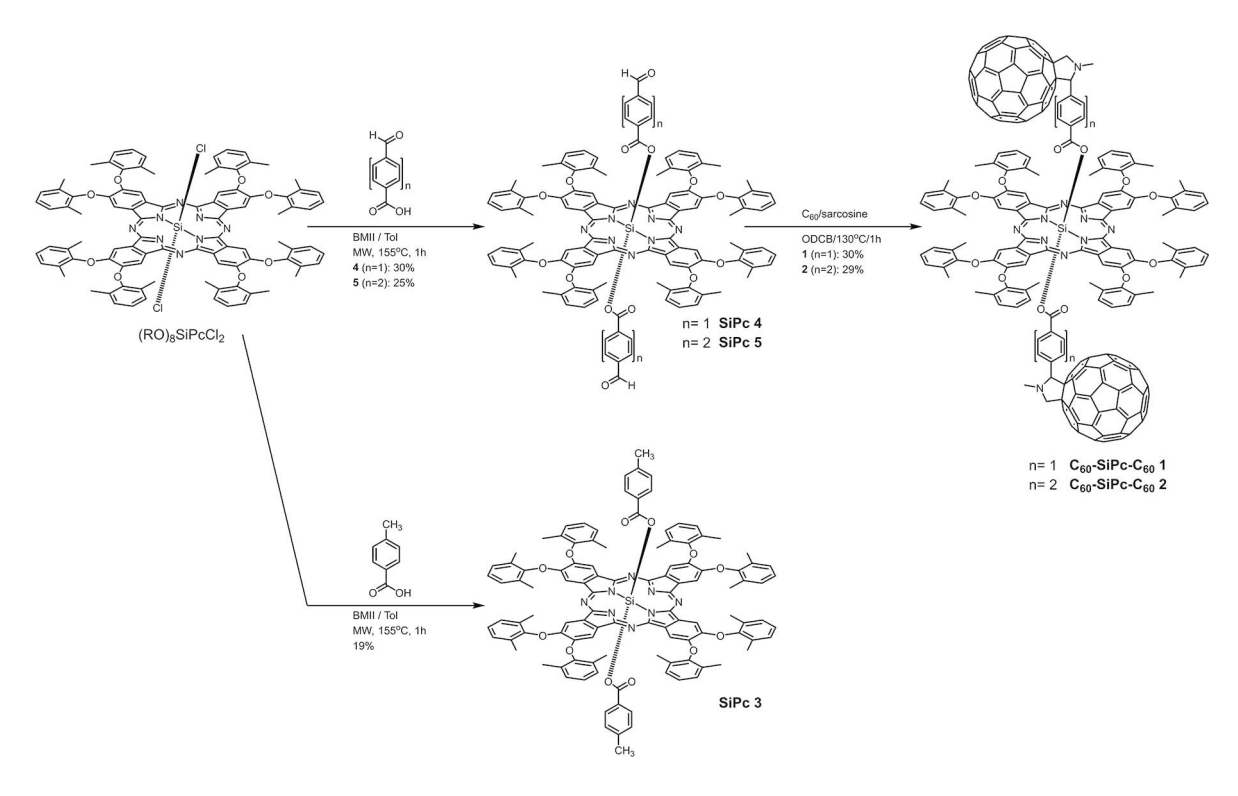
2.1. Syntheses

The axially substituted silicon phthalocyanines C₆₀-SiPc-C₆₀ 1 and C₆₀-SiPc-C₆₀ 2 were synthesized following the route described in Scheme 1. Starting from (RO)₈SiPcCl₂, which is firstly obtained from 5,6-bis(2,6-dimethylphenoxy)isoindoline-1,3-diimine and SiCl₄ (see SI), it is made to react for 1 h, under micro-wave irradiation (155°C,170 W) in a single-mode apparatus, with 3 equivalents of benzoic acid derivative, using dry toluene, as a solvent, and a catalytic amount of an ionic liquid,1-butyl-3-methylimidazolium iodide (BMII). This ionic liquid significantly improves the absorption of microwave radiation, so SiPcs 3-5 are obtained in about one hour, with yields ranging from 20 to 30%. These yields are comparable to those obtained in the preparation of similar compounds when a classical-heating method is employed and using long reaction times (> 12 h). [8,29,30,32,34,38,39] Finally, $\rm C_{60}\text{-}SiPc\text{-}C_{60}$ 1 and $\rm C_{60}\text{-}SiPc\text{-}C_{60}$ 2 are obtained through a double Prato's reaction, with sarcosine as nitrogen source and obtaining, both compounds, in a 29-30% yield. It is worth to note that, in this step, an excess of pristine C₆₀ is used and the reaction time is limited to 1 h, to minimize the formation of polyadducts. Thus, the obtained yields indicate an approximate efficiency of 55% for each cycloaddition, which is quite high for this type of reaction. This trend was previously observed by us during synthesis of different acceptor bearing PDI-SiPc-C₆₀ triads, whose final step was a Prato reaction. So we can infer that, in silicon phthalocyanine compounds bearing axial groups with aldehyde functionalities, phthalocyanine ring could provide an extra stabilization to the in situ generated azomethine ylide intermediates, which facilitates the following 1,3-dipolar cycloaddition to a C₆₀-fullerene [6,6] bond.

2.2. Characterization

All new compounds were characterized, at first, by ¹H NMR spectroscopy and High-resolution mass spectrometry (HR MALDI-TOF, See SI). All ¹H NMR spectra are clear and simple, with well-defined signals, and this is because silicon phthalocyanine compounds, axially and peripherally substituted with bulky groups, are soluble in a wide variety of organic solvents, presenting a very low tendency to aggregate in solution. Figure 2 shows, as an example, C₆₀-SiPc-C₆₀ 1 and 2 ¹H-NMR spectra, together with that of SiPc 3 (reference compound), registered in CDCl₃ at 25 °C. All of them show characteristic signals of their common structure, a peripherally octa-substituted phthalocyanine ring with 2,6-dimethylphenoxyl residues. These are, a sharp signal, centered at 8.26-8.24 ppm and corresponding to eight non-peripheral hydrogens, and two more signals assigned to peripheral substituents, a multiplet





Scheme 1. The synthetic route followed to obtain C_{60} -SiPc- C_{60} 1, C_{60} -SiPc- C_{60} 2, and SiPc 3.

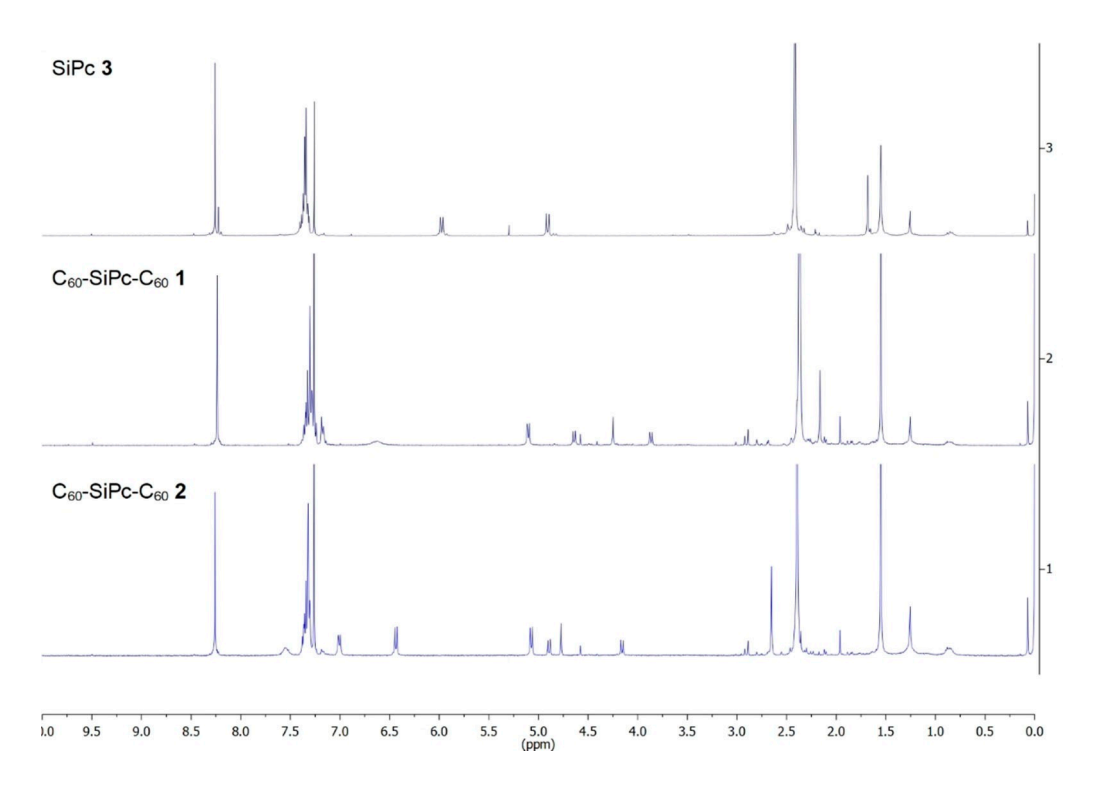


Figure 2. Comparison of SiPc 3 and C₆₀-SiPc-C₆₀ 1 and 2 ¹H NMR spectra in CDCl₃ as solvent at 25 °C.

which integrates for 24 aromatic hydrogens, centered around 7.42–7.27 ppm, and a singlet integrating for 48 hydrogens (16 \times CH₃) and centered at 2.37-2.42 ppm. Besides, it is also possible to appreciate signals ascribed to aromatic hydrogens of the

axial substituents, all of them peculiarly up-field shifted. This is caused by the influence of the ring current, generated while registering the spectra. For example, in the case of SiPc 3, these signals appear as two coupled doublets centered at 5.98 and



4.91 ppm, while equivalent hydrogens in C_{60} derivatives appear as two-two coupled signals, centered at 6.63 and 5.10 ppm in the case of 1, and centered at 7.55, 7.01, 6.44 and 5.07 ppm for 2. Here, the influence of C_{60} sphere is also observed, because *ortho* aromatic hydrogen signals, near to *N*-methylfulleropyrrolidinyl append, do not appear as doublets, but as broad singlets, due to restricted rotation of phenyl groups, [53] centered at 6.63 and 7.55 ppm, for C_{60} -SiPc- C_{60} 1 and 2, respectively.

2.3. Absorption and Fluorescence Spectroscopy, and Computational Studies

Figure 3a shows the absorption spectra, recorded in benzonitrile, of the phthalocyanines- C_{60} conjugates, C_{60} -SiPc- C_{60} 1 and 2, along with reference compounds and control. As it can be seen, all of them present phthalocyanine characteristic Soret and Q bands, around 360–370 nm and 700 nm region respec-

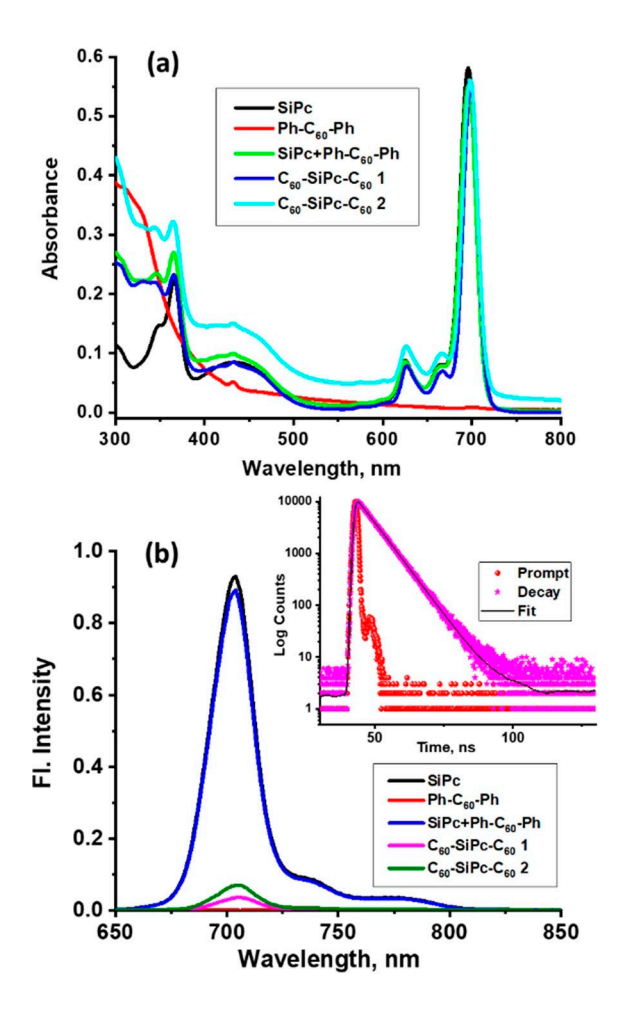


Figure 3. a) UV/Vis absorption spectroscopy normalized to the visible band, recorded in benzonitrile, of C_{60} -SiPc- C_{60} 1 and 2, SiPc, C_{60} control and 1:1 mixture of SiPc- C_{60} control. b) Fluorescence spectra, recorded in benzonitrile, of C_{60} -SiPc- C_{60} 1 and 2, SiPc, C_{60} control and 1:1 mixture of SiPc- C_{60} control. The samples were excited at 627 nm corresponding to the SiPc peak maxima. Inset in (b): The fluorescence decay profile of SiPc in benzonitrile from time correlated single photon counting method.

tively, plus an additional broad absorption, between 400 and 500 nm, attributed to an intramolecular charge-transfer complex between peripheral 2,6-dimethylphenoxyl substituents and phthalocyanine ring. The characteristic sharp peak of fulleropyrrolidine at 432 nm was also present in 1 and 2. Spectrum of 1 and 2 to that of the reference compound revealed a redshift in peak maxima, and an increase in the molar absorption coefficients due to the combined electronic and steric influence of the axial C₆₀-fullerene substituents. For example, if we focus on the Q-band, it is observed that the maximum wavelength moves from 696 nm of the reference SiPc (3 in Scheme 1) to 698 and 700 nm for 1 and 2, respectively. The electronic effect of the fullerene moiety in the ground state is apparent and more pronounced in the case of C₆₀-SiPc-C₆₀ 1, which has a shorter connector. The influence of fullerene on the intensity of the Q-band absorption maxima is also appreciated. Thus, the phthalocyanines C₆₀-SiPc-C₆₀ 1 and 2 show higher values than SiPc, and this is related to the volume of the axial substituents, as is also the case in the spectrum of 1:1 mixture of SiPc and C₆₀ control. That increase is, in this case, more pronounced for C₆₀-SiPc-C₆₀ 2, the one with the most voluminous axial substituents which indicates, therefore, a slightly lower tendency to aggregate.

Figure 3b shows the emission spectra of C₆₀-SiPc-C₆₀ 1 and 2, and of the controls, recorded in benzonitrile, employing 667 nm as excitation wavelength. In particular, SiPc 3 shows a medium-intensity fluorescence band centered at 704 nm, while both 1 and 2 show very low fluorescence (quenched by 96% and 93%, respectively, accompanied by a small red-shift of ~2 nm) compared to emission of either 3 or that of an equimolar control mixture of SiPc and C₆₀, indicating occurrence of excited state interactions between fullerene and phthalocyanine electroactive units. It is also worth to note that the emission band intensity decrease is a little bit more pronounced in the case of SiPc-C₆₀ 1, where the fullerene sphere is closer to the phthalocyanine core. Such quenching was absent in 1:1 physical mixture of SiPc and C₆₀-control. These emission measurements provide qualitative evidence of the photophysical behavior pursued with the molecular design of these dyads. That is, after selective irradiation of the phthalocyanine unit, the presence of the fullerene in these dyads offers a non-radiative deactivation path of the excited state, likely due to either electron or energy transfer events.

Lifetime of SiPc was evaluated from performing time correlated single photon counting (TCSPC) technique. The decay profile of SiPc in benzonitrile is shown in Figure 3b inset. Monoexponential decay with a lifetime of 6.11 ns ($\chi^2\!=\!1.05)$ was recorded. The observed monoexponential decays is suggestive of lack of aggregation formation of the phthalocyanine sensitizer utilized in the present study. Due to very low-fluorescence, no lifetime could be determined for compounds 1 and 2.

In order to estimate the distances between the donor and acceptor entities, and also to probe the electronic structure of 1 and 2, the compounds were optimized using B3LYP functional at 6-11G(d,p) basis set on *Gaussian 16.*^[54] Fully optimized structures of 1 and 2 are shown in Figure 4a and b. In the case

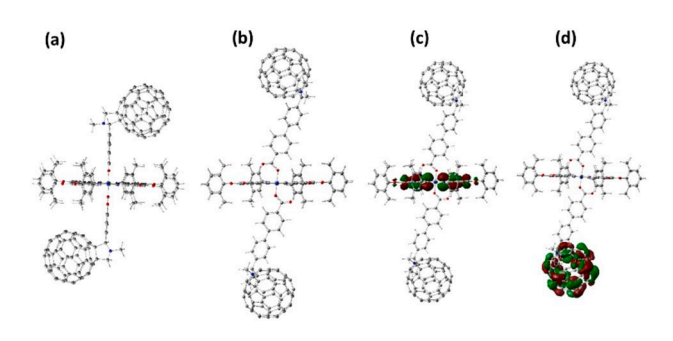
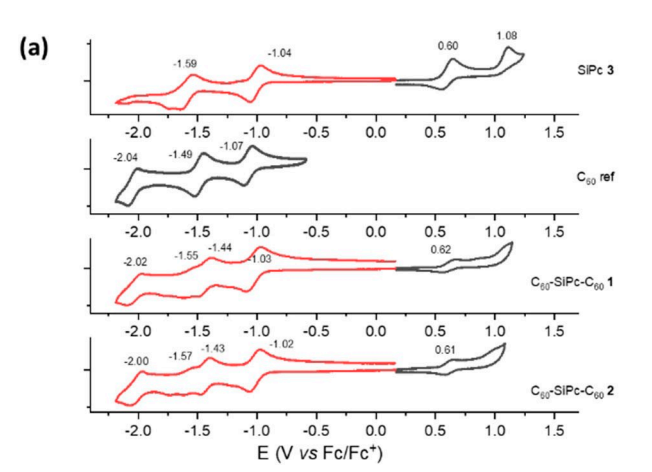


Figure 4. B3LYP/6-11G(d,p) optimized structure of (a) 1 and (b) 2. The frontier HOMO and LUMO of 2 is shown in (c) and (d), respectively. Similar HOMO and LUMOs were observed for compound 1.

of 1, Si–O bond length was 1.78 Å while the Si to center of C₆₀ distance was 11.56 Å. The center-to-center distance between the two C_{60} entities was 23.10 Å. In contrast, the distances measured for compound 2 revealed larger distances. That is, Sito-center of C₆₀ distance was 15.90 Å while the center-to-center distance between the two C₆₀ entities was 30.85 Å. Insertion of an additional phenyl ring in 2 increased the donor-acceptor distance by ~3.4 Å. The frontier orbitals generated on the optimized structures using GaussView^[55] program revealed their donor and acceptor properties, as shown in Figure 4c and d for compound 2. The first HOMO on the SiPc and first LUMO on C_{60} in the case of both 1 and 2 were witnessed, establishing their donor and acceptor characteristics within the dyads.

2.4. Electrochemistry, Free-Energy Calculations and Energy **Level Diagram**

Figure 5a shows the cyclic voltammograms (CVs) of C₆₀-SiPc-C₆₀ 1 and 2, SiPc 3, and N-methylfulleropyrrolidine (C₆₀-ref, see SI, reference), all of them recorded in benzonitrile and referenced to Fc/Fc⁺. Corresponding differential pulse voltammograms (DPVs) are shown in Figure S10. Oxidation and reduction potentials are also summarized in Table 1. The electronic influence of fullerene moieties on the electrochemical properties of C_{60} -SiPc- C_{60} 1 and 2 can be seen. Looking at the anodic part of registered voltammograms, we can see how the first oxidation potential (E_{ox}^{-1}) , centered at 0.60 V in the case of SiPc, moves to more positive values for C_{60} -SiPc- C_{60} 1 and 2, 0.62 and 0.61 V respectively (all reversible on CV time scale). Again, the electronic influence of C_{60} seems to be related to the distance to the phthalocyanine ring, and is, therefore, slightly more pronounced in the case of C_{60} -SiPc- C_{60} 1. On the other hand, first reduction waves of reference compounds, C₆₀-ref and SiPc 2, present close values, -1.07 and -1.04 V, while the second reduction of these two entities was separated by about 60 mV with values of $-1.49\,\mathrm{V}$ for C_{60} -ref, and $-1.55\,\mathrm{V}$ for SiPc , respectively. Consequently, the first reduction in the case of dyads 1 and 2 was an overlap of two processes involving SiPc and C_{60} electroreductions and was centered at $-1.03\,V$ for 1 and -1.02 V for 2, respectively. However, these waves were separated during the subsequent electroreduction wherein



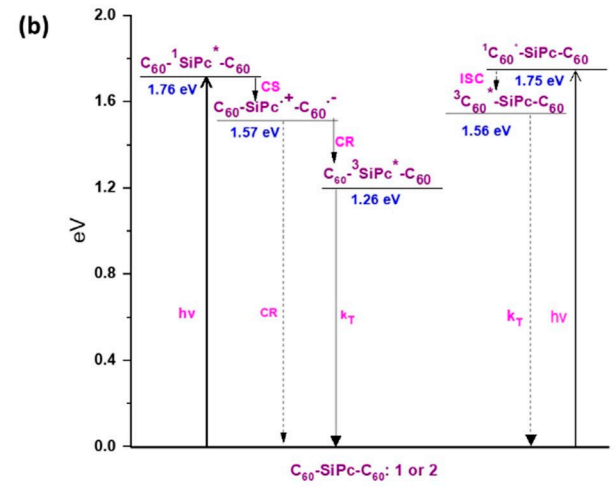


Figure 5. (a) Cyclic voltammograms, recorded in deaerated benzonitrile, containing 0.1 M Bu₄NPF₆, at a scan rate of 100 mV/s and referenced to Fc/ Fc⁺, of C₆₀-SiPc-C₆₀ 1 and 2, SiPc and C₆₀ ref compounds. (b) Energy level diagram showing possible photo-events in 1 and 2 in benzonitrile. Energy of the charge separated state in toluene is shown in the highlighted box. Solid arrow – most likely process, dashed arrow – less likely process. CS = charge separation, CR = charge recombination, and T = triplet emission.

Table 1. Redox potentials^[a] of C₆₀-SiPc-C₆₀ 1 and 2, and reference compounds, SiPc 3 and C₆₀ ref, in benzonitrile.

Compound	$E_{\rm red}^{-4}$	$E_{\rm red}^{3}$	$E_{\rm red}^{2}$	$E_{\rm red}^{-1}$	$E_{\rm ox}^{-1}$	E _{ox} ²
SiPc	_	-1.59	-	-1.04	0.60	1.08
C ₆₀ ref	-2.04	-	-1.49	-1.07	-	-
C ₆₀ -SiPc-C ₆₀ 1	-2.02	-1.55	-1.44	$-1.03^{[b]}$	0.62	-
C ₆₀ -SiPc-C ₆₀ 2	-2.00	-1.57	-1.43	$-1.02^{[b]}$	0.61	

[a] The half-wave potentials measured in V (vs. Fc/Fc+) are extracted from cyclic voltammograms of solutions in PhCN containing Bu₄NPF₆(0.10 M) as the supporting electrolyte. [b] Overlap of the first reductions of C₆₀ and

reduction of C₆₀ and SiPc was possible to observe as separate processes (reductions at -1.44 and -1.56 V in the case of 1 and -1.43 and -1.57 V in the case of **2**), thus confirming the existence of redox-active SiPc and C_{60} entities of the studied dyads, and the associated moderate degree of electronic perturbations modulating the redox potentials.



The feasibility of photoinduced electron transfer in these dyads was evaluated by performing free-energy change calculations according to Rehm and Weller. [56,57] Further, these freeenergy changes along with excited state energies were assembled to construct an energy level diagram as shown in Figure 5b. The ¹SiPc* formed by selective excitation of SiPc in both the triads could undergo, thermodynamically feasible direct electron transfer leading to SiPc*+-C₆₀*- charge-separated state with a stored energy of 1.57 eV in the charge separated state in benzonitrile. More than 90% quenching of the fluorescence emission is indicative of such charge-separated states. This charge-separated state could relax back to the ground state most likely via a 3SiPc* state positioned below that of the charge separated state at 1.26 eV. Small amounts of directly excited C_{60} could also promote charge separation leading to SiPc*+-C₆₀*- charge-separated state. In order to investigate these possible photoevents as a function of solvent polarity, transient absorption studies at different time scales were performed, as summarized in the following section.

2.5. Transient Pump-Probe Spectral Studies

First, femtosecond transient absorption (fs-TA) studies were carried out in polar benzonitrile and nonpolar toluene. Both the triads were excited at 698 nm corresponding to main visible peak of SiPc. Fs-TA spectral features of SiPc is shown in Figure S10a in the supporting information. Here, peaks at 623 nm and 698 nm due to the ground state bleaching (GSB) and stimulated emission(SE) and the positive peaks at 562, 645, 746, and 1270 nm were due to excited state absorption (ESA) were observed. Decay of singlet features were slow (Figure S10b) consistent with the earlier discussed fluorescence lifetime of SiPc.

Fs-TA spectra of compounds 1 and 2 in benzonitrile is shown in Figure 6a and c, respectively. In both cases, rapid decay and recovery of the ESA and GSB/SE peaks accompanied by diagnostic peak of $SiPc^{\bullet+}$ at 865 nm and of $C_{60}^{\bullet-}$ at 1010 nm providing direct evidence for formation of SiPc*+-C₆₀*- chargeseparated state. To analyze the transient data, decay associated spectra (DAS) were generated using global analysis, as shown in Figures 6b and d, respectively. Such data analysis of 1 generated three spectra; the first one at 14.3 ps had spectral features of ¹SiPc* (Figure 6b). The second spectrum at 374 ps revealed two negative peaks (representing growth) at the expected wavelengths of SiPc $^{\bullet+}$ at 865 nm and of $C_{60}^{\bullet-}$ at 1010 nm that could be attributed to the charge separated state. Using this time constant, the rate constant for charge separation, k_{CS} was determined and was found to be 2.7×10^9 s⁻¹. This value agreed well with earlier reported $k_{\rm CS}$ value for a similar dyad $(3.2 \times 10^9 \text{ s}^{-1})$, [48] however, in this case the SiPc had t-butyl groups at the ring periphery instead of the 2,6-dimethylphenoxyl groups. The third component with infinity time constant (>3 ns) revealed positive peaks at 865 and 1100 nm represented decay of the charge separated state. The infinity time constant suggests that the charge separated state lasts for over 3 ns.

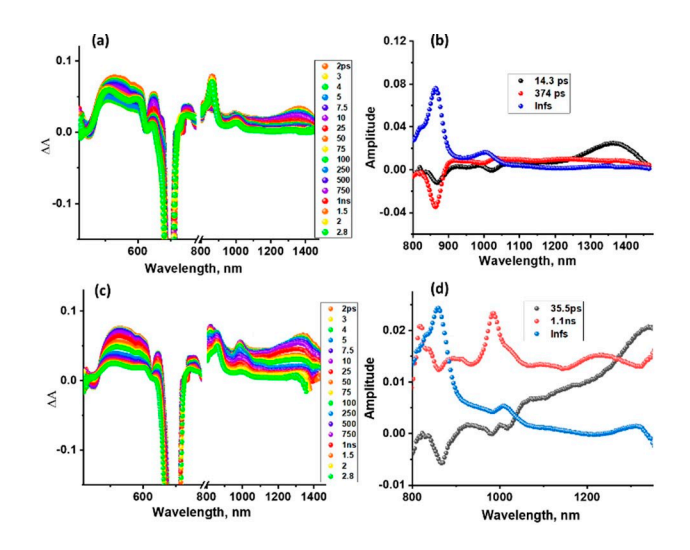


Figure 6. Femtosecond transient absorption spectra at the indicated delay times of (a) 1 and (b) 2 in deaerated benzonitrile (λ_{ex} = 698 nm). Decay associated spectra from global analysis are shown in (b) and (d), respectively for 1 and 2.

To verify whether a long-lived charge separated state does exist in case of 1, nanosecond transient absorption (ns-TA) spectral measurements were carried out as shown in Figure 7a. Spectral features were typical of that of the 3SiPc* (see Figure S11 for SiPc ns-TA spectra) with a broad signal centered around 535 nm. No peaks in the near-IR region corresponding to either $SiPc^{\bullet+}$ or $C_{60}^{\bullet-}$ were present. This signal decayed with a time constant of 82 µs that compared with a time constant of 88 µs recorded for pristine SiPc recorded under similar experimental conditions. Energy level diagram in Figure 5b predicted the SiPc*+-C₆₀*- charge separated state to populate the lowlying 3SiPc* state and such a competition would reduce the lifetime of the charge separated state. This seems to be the

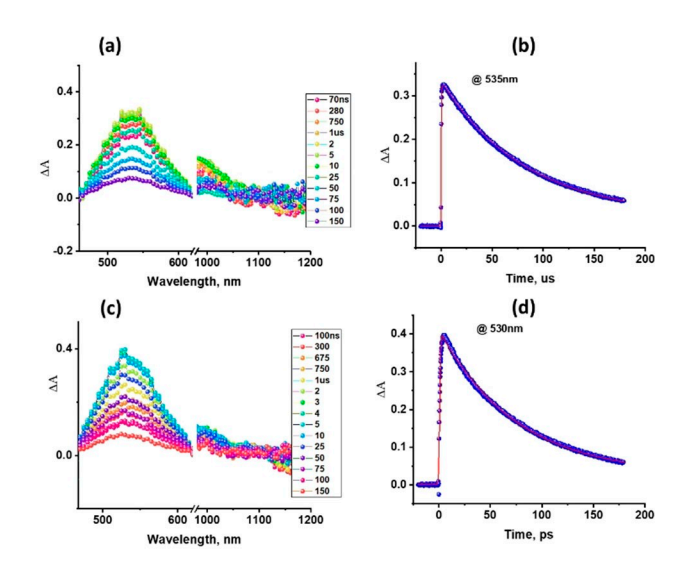


Figure 7. Nanosecond transient absorption spectra at the indicated delay times of (a) 1 and (b 2 in deaerated benzonitrile (λ_{ex} = 435 nm). Time profile of the 535 nm band is shown in (b) and (d), respectively for 1 and 2.



case here where the final lifetime of charge separated species could be between 3-20 ns (20 ns is the lower detection limit of our ns-TA setup).

The DAS generated for compound 2 was almost similar to that of 1. The analysis also resulted in three spectra, the first of which with a time constant of 35.5 ps had features of ¹SiPc* along with developing peaks of SiPc*+-C₆₀*- charge separated state (and some 1C60* state). The 1.1 ns revealed features of developing charge separated state (Figure 6d). The rate constant for charge separation, k_{CS} , determined using this time constant was found to be $9.1 \times 10^8 \,\mathrm{s}^{-1}$, about 3.7 times slower than that observed for 1 due to longer donor-acceptor distance. The DAS with infinity time constant was typical of that of the decaying charge separated state. In this case too, ns-TA spectra were recorded as shown in Figure 7b, which also revealed spectra corresponding ³SiPic* (lifetime of 72 μs), as predicted by Figure 5b. In this case also, it is safer to say that the final lifetime of charge separated species lies between 3-20 ns.

3. Conclusions

In summary, the present study brings out the importance of distance between donor-acceptor entities in multichromophoric conjugates in governing the excited state electron transfer events. In the case of $C_{60}\mbox{-SiPc-}C_{60}$ 1 where the SiPc and C_{60} are separated by a phenyl spacer, faster electron transfer was observed with k_{cs} around $2.7 \times 10^9 \, \mathrm{s}^{-1}$ in benzonitrile. However, in the case of C_{60} -SiPc- C_{60} 2, a slower rate of electron transfer with k_{cs} equal to $9.1 \times 10^8 \,\mathrm{s}^{-1}$ was observed due to increased donor-acceptor distance. The addition of an extra phenyl spacer revealed a significant effect on the rate of electron transfer. The charge separated state lasted over 3 ns in both cases, however, ns-TA studies revealed spectra corresponding to ³SiPc* and not that of a charge separated state. As predicted from the energy level diagram, the charge separated states populated the lowlying SiPc triplet state prior returning to the ground state.

Experimental Section

Chemicals

All reagents used for synthesis and spectroscopic studies were analytical grade and are used as received. Microwave irradiation was performed in a Discover® CEM monomode instrument.

Spectral, Electrochemical, and Photophysical Measurements

NMR spectra were measured with a Bruker AC 300. Mass spectra were obtained from a Bruker Microflex matrix-assisted laser desorption/ionization time of flight (MALDI-TOF).

UV/Vis spectra were recorded either on a Helios Gamma spectrophotometer or a Shimadzu Model 2550 double-monochromator. Fluorescence spectra were recorded either on a Perkin-Elmer LS 55 luminescence spectrometer or Horiba Yvon Nanolog coupled with time-correlated single-photon counting with nanoLED excitation sources. A right-angle detection method was used to record fluorescence emission

Cyclic (CV) and differential pulse voltammetry (DPV, see SI) measurements were performed at 298 K in a conventional threeelectrode cell using a m-AUTOLAB type III potentiostat/galvanostat. CVs and DPVs were performed at 100 mV/s and 20 mV/s scan rates, respectively. Sample solutions (ca. 0.5 mM) were prepared in deaerated PhCN, containing 0.10 M tetrabutylammonium hexafluorophosphate (TBAPF₆) as supporting electrolyte. A glassy carbon (GC) working electrode, an Ag/AgNO₃ reference electrode, and a platinum wire counter electrode were used. Ferrocene/ferrocenium was the internal standard for all measurements.

Femtosecond transient absorption spectroscopy experiments were performed using an ultrafast femtosecond laser source (Libra) by Coherent incorporating a diode-pumped, modelocked Ti:sapphire laser (Vitesse) and a diode-pumped intracavity doubled Nd:YLF laser (Evolution) to generate a compressed laser output of 1.45 W. For optical detection, a Helios transient absorption spectrometer coupled with a femtosecond harmonics generator, both provided by Ultrafast Systems LLC, was used. The sources for the pump and probe pulses were derived from the fundamental output of Libra (Compressed output 1.45 W, pulse width 100 fs) at a repetition rate of 1 kHz; 95% of the fundamental output of the laser was introduced into a TOPAS-Prime-OPA system with a 290-2600 nm tuning range from Altos Photonics Inc., (Bozeman, MT), while the rest of the output was used for generation of a white light continuum. Kinetic traces at appropriate wavelengths were assembled from the time-resolved spectral data. Data analysis was performed using Surface Xplorer software supplied by Ultrafast Systems. All measurements were conducted in degassed solutions at 298 K. The estimated error in the reported rate constants is \pm 10 %.

The nanosecond transient absorption measurement was done using laser flash photolysis instrumental setup composed of an Opolette HE 355 LD pumped by a high-energy Nd:YAG laser with second and third harmonics OPO (tuning range 410-2200 nm, pulse repetition rate 20 Hz, pulse length 7 ns) with laser powers of 1.0-3 mJ/pulse. For spectral measurements, a Proteus UV-vis-NIR flash photolysis spectrometer (Ultrafast Systems, Sarasota, FL) with a fiberoptic delivered white light as the probe and either a fast rise Si photodiode detector (covering 200-1000 nm range) or an InGaAs photodiode detector (covering 900-1600 nm range) was used. The output from the photodiodes and a photomultiplier tube was recorded using a digitizing Tektronix oscilloscope. Data analysis was performed using Surface Xplorer software from Ultrafast Systems.

Synthesis and Characterization of New Compounds

Synthesis of (RO)₈SiPcCl₂

A suspension of 500 mg of 5,6-bis(2',6'-dimethylphenoxyl)-1,3diiminoisoindoline (1.30 mmol), 5 mL of dry quinoline and 0.5 mL of SiCl₄ is kept refluxed for one hour under inert atmosphere and avoiding light. After that, the mixture reaches room temperature and is precipitated over 100 ml of dry acetone. Finally, vacuum filtration affords 510 mg of product (quant) as a greenish solid, which is used in successive reactions without additional purification. UV-Vis (CHCl₃) λ_{max}/nm : 377, 634, 706.



Synthesis of SiPc 4

A suspension of $(RO)_8SiPcCl_2$ (50 mg, 0.032 mmol), 4-carboxybenzal-dehyde (24 mg, 0.159 mmol), one drop of 1-butyl-3-methylimidazolium iodide (BMII) and 5 mL of dry toluene is prepared in an 8 mL microwave tube. The mixture is then held at a constant temperature of 155 °C for one hour, using a microwave reactor (170 W). After that, the crude reaction reaches 60 °C, then diluted with toluene and washed with NaOH 1 M, H₂O, and brine. Finally, 17 mg of pure compound (30%) were obtained, as a light green solid, after column chromatographic purification (neutral Al₂O₃, Hx \rightarrow Hx/CH₂Cl₂ 1:2 v/v). ¹H-NMR (300 MHz, CDCl₃, 25 °C): δ = 9.39 (2H, s, H-CHO), 8.29 (8H, m, H-Pc), 7.43–7.30 (24H, br s, H-Ar), 6.71 (4H, d, J=8.2 Hz, H-Ar), 5.19 (4H, d, J=8.2 Hz, H-Ar), 2.41 (48H, s, 16×CH3). HR-MS (MALDI-TOF, dithranol): m/z [M⁺] calculated for C₁₁₂H₉₀N₈O₁₄Si 1799.6379, found 1799.6539. UV-Vis (CHCl₃) λ max/nm (logɛ): 365 (4.94), 439 (4.56), 629 (4.58), 667 (4.55), 701 (5.45).

Synthesis of SiPc 5

A suspension of (RO)₈SiPcCl₂ (100 mg, 0.064 mmol), 4-(4'-formylphenyl)benzoic acid (43 mg, 0.19 mmol), one drop of 1-butyl-3methylimidazolium iodide (BMII) and 5 mL of dry toluene is prepared in an 8 mL microwave tube. The mixture is then held at a constant temperature of 155 °C for one hour, using a microwave reactor (170 W). After that, the crude reaction reaches 60°C, then diluted with toluene and washed with NaOH 1 M, H₂O, and brine. Finally, 25 mg of pure compound (25%) were obtained, as a light green solid, after column chromatographic purification (neutral Al_2O_3 , $Hx \rightarrow Hx/CH_2Cl_2$ 1:2v/v). ¹H-RMN (300 MHz, CDCl₃, 25 °C): $\delta =$ 9.86 (2H, s, CHO), 8.30 (8H, m, H-Pc), 7.63 (4H, d, H-Ar), 7.34 (24H, br s, H-Ar), 7.10 (4H, d, H-Ar), 6.48 (4H, d, H-Ar), 5.16 (4H, d, H-Ar), 2.42 (48H, s, 16×CH₃). HR-MS (MALDI-TOF, dithranol): m/z [M⁺] calculated for C₁₂₄H₉₈N₈O₁₄Si 1951.7005, found 1951.6916. UV-Vis (CHCl₃) λ_{max}/nm (log ϵ): 365 (4.92), 437 (4.51), 627 (4.55), 666 (4.51), 699 (5.42).

Synthesis of SiPc 3

A suspension of (RO) $_8$ SiPcCl $_2$ (50 mg, 0.032 mmol), 4-methylbenzoic acid (36 mg, 0.264 mmol), one drop of 1-butyl-3-methylimidazolium iodide (BMII) and 5 mL of dry toluene is prepared in an 8 mL microwave tube. The mixture is then held at a constant temperature of 155 °C for one hour, using a microwave reactor (170 W). After that, the crude reaction reaches 60 °C, diluted with toluene and washed with NaOH 1 M, H $_2$ O and brine. Finally, 11 mg of pure compound (19%) were obtained, as a light green solid. 1 H-RMN (300 MHz, CDCl $_3$, 25 °C): δ =8.26 (8H, s, H-Pc), 7.42–7.30 (24H, m, H-Ar), 5.98 (4H, d, J=8.1 Hz, H-Ar), 4.91 (4H, d, J=8.1 Hz, H-Ar), 2.42 (48H, s, $16\times$ CH $_3$), 1.68 (6H, s, $2\times$ CH $_3$) ppm. HR-MS (MALDI-TOF, dithranol): m/z [M-H] $^-$ calculated for C $_{112}$ H $_{94}$ N $_8$ O $_{12}$ Si 1770.6789, found 1770.6798. UV-Vis (CHCl $_3$) λ_{max} /nm (log $_8$): 365 (4.72), 437 (4.33), 625 (4.33), 662 (4.27), 696 (5.15).

Synthesis of C_{60} -SiPc- C_{60} 1

20 mg (0.011 mmol) of SiPc 4, 8 mg of sarcosine (0.090 mmol) and 25 mg of C_{60} (0.035 mmol) were dissolved in 3 ml of o-dichlorobenzene. The mixture was heated at 130 °C for one hour under an inert atmosphere. Evaporation of the solvent gave a crude product which was finally purified by column chromatography (Al_2O_3 , Hexane/Toluene) to afford 11 mg (30%) of the pure compound as a brown-green powder. 1 H-RMN (300 MHz, CDCl $_3$, 25 °C): δ = 8.24 (8H, s, H-Pc), 7.40–7.27 (24H, m, H-Ar), 6.63 (4H, br s, H-Ar), 5.10 (4H, d, J=8.6 Hz, H-Ar), 4.64 (2H, d, J=9.5 Hz, H-Pyrrolidine), 4.25 (2H, s, H-

Pyrrolidine), 3.87 (2H, d, J=9.5 Hz, H-Pyrrolidine), 2.37 (48H, s, $16\times$ CH₃), 2.16 (6H, s, $2\times$ N-CH₃) ppm. HR MS (MALDI-TOF, dithranol): m/z [M-H]⁻ calculated for C₂₃₆H₁₀₁N₁₀O₁₂Si 3295.7398, found 3295.7414. UV-Vis (CHCl₃) λ_{max} /nm (logɛ): 364 (4.89), 433 (4.49), 627 (4.42), 665 (4.35), 700 (5.24).

Synthesis of C₆₀-SiPc-C₆₀ 2

20 mg (0.01 mmol) of SiPc **5**, 7.17 mg of sarcosine (0.081 mmol), and 23 mg of C_{60} (0.032 mmol) were dissolved in 2.9 ml of odichlorobenzene. The mixture was heated at 130 °C for one hour under an inert atmosphere. Evaporation of the solvent gave a crude product which was finally purified by column chromatography (Al₂O₃, Hexane/Toluene) to afford 10 mg (29%) of the pure compound as a brown green powder. ¹H-RMN (300 MHz, CDCl₃, 25 °C): δ =8.26 (8H, s, H-Pc), 7.55 (4H, br s, H-Ar), 7.41–7.28 (24H, m, H-Ar), 7.01 (4H, d, J=8.0 Hz, H-Ar), 6.44 (4H, d, J=8.5 Hz, H-Ar), 5.07 (4H, d, J=8.5 Hz, H-Ar), 4.89 (2H, d, J=9.6 Hz, H-Pyrrolidine), 4.77 (2H, s, H-Pyrrolidine), 4.16 (2H, d, J=9.6 Hz, H-Pyrrolidine), 2.65 (6H, s, 2×N-CH₃), 2.37 (48H, s, 16×CH₃) ppm. HR MS (MALDI-TOF, dithranol): m/z [M-H]⁻ calculated for C₂₄₈H₁₁₀N10O₁₂Si 3447.8028, found 3447.8045. UV-Vis (CHCl₃) λ_{max} /nm (logε): 364 (4.90), 436 (4.45), 626 (4.40), 664 (4.35), 698 (5.27)

Acknowledgements

This material is based upon work supported by the National Science Foundation under Grant Nos. 1401188 and 2000988 to FD, and by the Ministerio de Ciencia e Innovación of Spain and FEDER funds under Grants CTQ2017-87102-R and RED2018-102471-T to ASS. Computational work was performed at the Holland Computing Center of the University of Nebraska, which receives support from the Nebraska Research Initiative.

Conflict of Interest

The authors declare no conflict of interest.

Keywords: axial binding motif • energy transfer • fullerene • photoinduced charge separation • phthalocyanines

- [1] A. C. Benniston, A. Harriman, *Mater. Today* 2008, 11, 26–34.
- [2] M. E. El-Khouly, E. El-Mohsnawy, S. Fukuzumi, J. Photochem. Photobiol. C 2017, 31, 36–83.
- [3] J. D. Megiatto Jr, A. Antoniuk-Pablant, B. D. Sherman, G. Kodis, M. Gervaldo, T. A. Moore, A. L. Moore, D. Gust, *Proc. Natl. Acad. Sci. USA* 2012, 109, 15578–15583, S15578/1-S15578/31.
- [4] P. Xue, Q. Xu, P. Gong, C. Qian, Z. Zhang, J. Jia, X. Zhao, R. Lu, A. Ren, T. Zhang, RSC Adv. 2013, 3, 26403–26411.
- [5] F. Scarel, C. Ehli, D. M. Guldi, A. Mateo-Alonso, Chem. Commun. (Camb.) 2013, 49, 9452–9454.
- [6] P. Mondal, A. Chaudhary, S. P. Rath, *Dalton Trans.* 2013, 42, 12381–12394.
- Y. Wu, Y. Zhen, Z. Wang, H. Fu, J. Phys. Chem. A 2013, 117, 1712–1720.
 C. B. KC, G. N. Lim, V. N. Nesterov, P. A. Karr, F. D'Souza, Chem. Eur. J. 2014, 20, 17100–17112.
- [9] S. K. Das, A. Mahler, A. K. Wilson, F. D'Souza, ChemPhysChem 2014, 15, 2462–2472.
- [10] S. K. Das, B. Song, A. Mahler, V. N. Nesterov, A. K. Wilson, O. Ito, F. D'Souza, J. Phys. Chem. C 2014, 118, 3994–4006.



- [11] P. Damlin, M. Haetoenen, S. E. Dominguez, T. Aeaeritalo, H. Kivelae, C. Kvarnstroem, RSC Adv. 2014, 4, 8391-8401.
- [12] O. Trukhina, M. Rudolf, G. Bottari, T. Akasaka, L. Echegoyen, T. Torres, D. M. Guldi, J. Am. Chem. Soc. 2015, 137, 12914-12922.
- K. Sudhakar, S. Gokulnath, L. Giribabu, G. N. Lim, T. Trâm, F. D'Souza, Chem. Asian J. 2015, 10, 2708-2719.
- [14] L. Martin-Gomis, G. Rotas, K. Ohkubo, F. Fernández-Lázaro, S. Fukuzumi, N. Tagmatarchis, Á. Sastre-Santos, Nanoscale 2015, 7, 7437-7444.
- [15] M. Sekita, A. J. Jimenez, M. L. Marcos, E. Caballero, M. S. Rodriguez-Morgade, D. M. Guldi, T. Torres, Chem. Eur. J. 2015, 21, 19028-19040.
- G. Rotas, L. Martín-Gomis, K. Ohkubo, F. Fernández-Lázaro, S. Fukuzumi, N. Tagmatarchis, Á. Sastre-Santos, Chem. Eur. J. 2016, 22, 15137-15143.
- [17] G. N. Lim, C. O. Obondi, F. D'Souza, Angew. Chem. Int. Ed. 2016, 55, 11517-11521; Angew. Chem. 2016, 128, 11689-11693.
- [18] G. D. Blanco, A. J. Hiltunen, G. N. Lim, C. B. KC, K. M. Kaunisto, T. K. Vuorinen, V. N. Nesterov, H. J. Lemmetyinen, F. D'Souza, ACS Appl. Mater. Interfaces 2016, 8, 8481-8490.
- N. Zarrabi, C. Agatemor, G. N. Lim, A. J. Matula, B. J. Bayard, V. S. Batista, F. D'Souza, P. K. Poddutoori, J. Phys. Chem. C 2019, 123, 131-143.
- [20] A. Gouloumis, F. Oswald, M. E. El-Khouly, F. Langa, Y. Araki, O. Ito, Eur. J. Org. Chem. 2006, 2006, 2344-2351.
- [21] D. Gust, T. A. Moore, A. L. Moore, Acc. Chem. Res. 2001, 34, 40-48.
- [22] G. de la Torre, C. G. Claessens, T. Torres, Chem. Commun. 2007, 2000-2015.
- [23] H. Imahori, T. Umeyama, S. Ito, Acc. Chem. Res. 2009, 42, 1809-1818.
- N. Martín, L. Sánchez, B. Illescas, I. Pérez, Chem. Rev. 1998, 98, 2527-
- [25] M. Lederer, D. M. Guldi, M. Ince, M. V. Martinez-Diaz, T. Torres, T. Torres, ChemPlusChem 2016, 81, 941-946.
- [26] M. Niemi, N. V. Tkachenko, A. Efimov, H. Lehtivuori, K. Ohkubo, S. Fukuzumi, H. Lemmetyinen, J. Phys. Chem. A 2008, 112, 6884-6892.
- A. de la Escosura, M. V. Martinez-Diaz, T. Torres, R. H. Grubbs, D. M. Guldi, H. Neugebauer, C. Winder, M. Drees, N. S. Sariciftci, Chem. Asian J. 2006, 1, 148-154.
- [28] R. Kaur, F. Possanza, F. Limosani, S. Bauroth, R. Zanoni, T. Clark, G. Arrigoni, P. Tagliatesta, D. M. Guldi, J. Am. Chem. Soc. 2020, 142, 7898-
- [29] M. Wolf, J. I.T. Costa, M. B. Minameyer, T. Drewello, A. C. Tome, D. M. Guldi, J. Phys. Chem. C 2019, 123, 28093-28099.
- [30] A. J. Stasyuk, O. A. Stasyuk, M. Sola, A. A. Voityuk, Phys. Chem. Chem. Phys. 2019, 21, 25098-25107.
- [31] Z.-Y. Wu, N. Zhang, S.-Y. Yang, L.-J. Huang, Fullerenes Nanotubes Carbon Nanostruct. 2019, 27, 853-863.
- [32] E. Regulska, D. M. Rivera-Nazario, J. Karpinska, M. E. Plonska-Brzezinska, L. Echegoyen, Molecules 2019, 24, 1118.
- [33] V. Nikolaou, F. Plass, A. Planchat, A. Charisiadis, G. Charalambidis, P. A. Angaridis, A. Kahnt, F. Odobel, A. G. Coutsolelos, Phys. Chem. Chem. Phys. 2018, 20, 24477-24489.
- [34] Y. Chen, M. E. El-Khouly, M. Sasaki, Y. Araki, O. Ito, Org. Lett. 2005, 7, 1613-1616.
- [35] P. K. Poddutoori, G. N. Lim, A. S.D. Sandanayaka, P. A. Karr, O. Ito, F. D'Souza, M. Pilkington, A. van der Est, Nanoscale 2015, 7, 12151-12165.
- P. K. Poddutoori, L. P. Bregles, G. N. Lim, P. Boland, R. G. Kerr, F. D'Souza, Inorg. Chem. 2015, 54, 8482-8494.
- [37] N. Zarrabi, S. Seetharaman, S. Chaudhuri, N. Holzer, V. S. Batista, A. van der Est, F. D'Souza, P. K. Poddutoori, J. Am. Chem. Soc. 2020, 142, 10008-10024.
- [38] K. N. Kim, C. S. Choi, K.-Y. Kay, Tetrahedron Lett. 2005, 46, 6791-6795.
- [39] A. Mateo-Alonso, C. Sooambar, M. Prato, Comptes Rendus Chim. 2006, 9, 944-951.
- [40] S. Fukuzumi, T. Honda, K. Ohkubo, T. Kojima, Dalton Trans. 2009, 3880-3889.
- [41] M. S. Rodriguez-Morgade, M. E. Plonska-Brzezinska, A. J. Athans, E. Carbonell, G. de Miguel, D. M. Guldi, L. Echegoyen, T. Torres, J. Am. Chem. Soc. 2009, 131, 10484-10496.
- P. K. Poddutoori, G. N. Lim, M. Pilkington, F. D'Souza, A. van der Est, Inorg. Chem. 2016, 55, 11383-11395.
- [43] A. Bagaki, H. B. Gobeze, G. Charalambidis, A. Charisiadis, C. Stangel, V. Nikolaou, A. Stergiou, N. Tagmatarchis, F. D'Souza, A. G. Coutsolelos, Inorg. Chem. 2017, 56, 10268-10280.
- [44] G. N. Lim, S. Hedström, K. A. Jung, P. A.D. Smith, V. S. Batista, F. D'Souza, A. van der Est, P. K. Poddutoori, J. Phys. Chem. C 2017, 121, 14484-14497.

- [45] N. Zarrabi, C. O. Obondi, G. N. Lim, S. Seetharaman, B. G. Boe, F. D'Souza, P. K. Poddutoori, Nanoscale 2018, 10, 20723-20739.
- [46] L. Martin-Gomis, K. Ohkubo, F. Fernández-Lázaro, S. Fukuzumi, Á. Sastre-Santos, J. Phys. Chem. C 2008, 112, 17694-17701.
- F. J. Céspedes-Guirao, L. Martin-Gomis, K. Ohkubo, S. Fukuzumi, F. Fernández-Lázaro, Á. Sastre-Santos, Chem. Eur. J. 2011, 17, 9153-63.
- [48] L. M. Arellano, L. Martín-Gomis, H. B. Gobeze, M. Barrejón, D. Molina, M. J. Gómez-Escalonilla, J. L.G. Fierro, M. Zhang, M. Yudasaka, S. lijima, F. D'Souza, F. Langa, A. Sastre-Santos, J. Mater. Chem. C 2015, 3, 10215-10224.
- [49] L. Martín-Gomis, K. Ohkubo, F. Fernández-Lázaro, S. Fukuzumi, Á. Sastre-Santos, Org. Lett. 2007, 9, 3441-3444.
- [50] L. Martín-Gomis, K. Ohkubo, F. Fernández-Lázaro, S. Fukuzumi, Á. Sastre-Santos, Chem. Commun. 2010, 46, 3944.
- L. Martín-Gomis, F. Peralta-Ruiz, M. B. Thomas, F. Fernández-Lázaro, F. D'Souza, Á. Sastre-Santos, Chem. Eur. J. 2017, 23, 3863-3874.
- [52] L. Martín-Gomis, R. Díaz-Puertas, S. Seetharaman, P. A. Karr, F. Fernández-Lázaro, F. D'Souza, Á. Sastre-Santos, Chem. Eur. J. 2020, 26, 4822-4832.
- [53] P. de la Cruz, A. de la Hoz, L. M. Font, F. Langa, M. C. Pérez-Rodríguez, Tetrahedron Lett. 1998, 39, 6053-6056.
- Gaussian 16, Revision A.03, M. J. Frisch, G. W. Trucks, H. B. Schlegel, G. E. Scuseria, M. A. Robb, J. R. Cheeseman, G. Scalmani, V. Barone, G. A. Petersson, H. Nakatsuji, X. Li, M. Caricato, A. V. Marenich, J. Bloino, B. G. Janesko, R. Gomperts, B. Mennucci, H. P. Hratchian, J. V. Ortiz, A. F. Izmaylov, J. L. Sonnenberg, D. Williams-Young, F. Ding, F. Lipparini, F. Egidi, J. Goings, B. Peng, A. Petrone, T. Henderson, D. Ranasinghe, V. G. Zakrzewski, J. Gao, N. Rega, G. Zheng, W. Liang, M. Hada, M. Ehara, K. Toyota, R. Fukuda, J. Hasegawa, M. Ishida, T. Nakajima, Y. Honda, O. Kitao, H. Nakai, T. Vreven, K. Throssell, J. A. Montgomery, Jr., J. E. Peralta, F. Ogliaro, M. J. Bearpark, J. J. Heyd, E. N. Brothers, K. N. Kudin, V. N. Staroverov, T. A. Keith, R. Kobayashi, J. Normand, K. Raghavachari, A. P. Rendell, J. C. Burant, S. S. Iyengar, J. Tomasi, M. Cossi, J. M. Millam, M. Klene, C. Adamo, R. Cammi, J. W. Ochterski, R. L. Martin, K. Morokuma, O. Farkas, J. B. Foresman, D. J. Fox, Gaussian, Inc., Wallingford CT, 2016.
- GaussView, Version 6.0.16, Roy Dennington, T. A. Keith, J. M. Millam, Semichem Inc., Shawnee Mission, KS, 2016.
- [56] D. Rehm, A. Weller, Isr. J. Chem. 1970, 8, 259-271.
- The free energy change for charge separation (ΔG_{CS}) from the singlet excited state ¹SiPc* within the donor-acceptor system is calculated in benzonitrile using spectroscopic, computational and electrochemical data following Equations (1-3).

$$-\Delta G_{CR} = E_{ox} - E_{red} + \Delta G_{S}$$
 (1)

$$-\Delta G_{CS} = \Delta E_{00} - (-\Delta G_{CR}) \tag{2}$$

where ΔE_{00} and ΔG_{CS} correspond to the energy of excited singlet state and electrostatic energy, respectively. The E_{ox} and E_{red} represent the oxidation potential of the electron donor (SiPc) and the reduction potential of the electron acceptor, C_{60} . The term ΔGs refers to the static Coulombic energy, calculated by using the "dielectric continuum model" according to Equation (3):

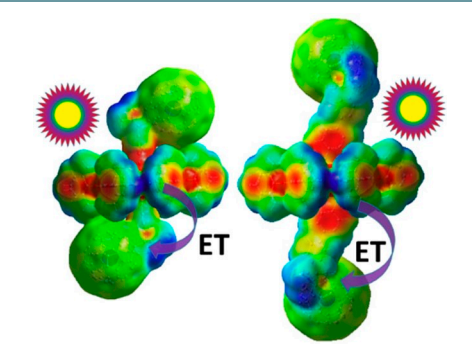
$$\Delta G_s = \frac{e^2}{4\pi\varepsilon_0} \left[\left(\frac{1}{2R_+} + \frac{1}{2R_-} \right) \Delta \left(\frac{1}{\varepsilon_R} \right) - \frac{1}{R_{CC}\varepsilon_R} \right]$$
 (3)

The symbols ε_0 , and ε_R represent vacuum permittivity and dielectric constant (26 and 2.38, respectively for benzonitrile and toluene) of the solvent used for photochemical and electrochemical studies, respectively. R_{CC} is the center-to-center distance between SiPc and C_{60} being 11.56 Å for 1 and 15.90 Å for 2, respectively. The symbols R_{+} and R_{-} (6.55 Å for SiPc, and 3.6 Å from computed structure) refer to radii of the cation and anion species, respectively.

Manuscript received: July 6, 2020 Revised manuscript received: July 29, 2020 Accepted manuscript online: July 30, 2020 Version of record online: ■■,

ARTICLES

Distance Matter: The effect of donor-acceptor distance in governing the kinetics of electron transfer is demonstrated in axially linked silicon phthalocyanine-C₆₀ dyads using time-resolved transient absorption studies operating at different time scales.



Dr. L. Martín-Gomis, S. Seetharaman, D. Herrero, Prof. Dr. P. A. Karr, Prof. Dr. F. Fernández-Lázaro, Prof. Dr. F. D'Souza*, Prof. Dr. Á. Sastre-Santos*

1 – 10

Distance-Dependent Electron Transfer Kinetics in Axially Connected Silicon Phthalocyanine-Fullerene Conjugates

